Simulations of satellites mock-up fragmentation

Lorenzo Olivieri[a]*, Cinzia Giacomuzzo[b], Alessandro Francesconi[c]

[a] *CISAS G. Colombo, University of Padova, Via Venezia 15, 35131 Padova PD, Italy,* lorenzo.olivieri@unipd.it

[b] *DII, University of Padova, Via Venezia 1, 35131 Padova PD, Italy,* cinzia.giacomuzzo@unipd.it

[c] *DII/CISAS G. Colombo, University of Padova, Via Venezia 1, 35131 Padova PD, Italy,* alessandro.francesoni@unipd.it

* Corresponding Author

Abstract

High energy in-space collisions may lead to the catastrophic fragmentation of entire spacecraft. Current empirical models employed to predict spacecraft breakup are based on ground experiments and observation of debris cloud generated by collision events. Due to the continuous growth of the number of resident objects orbiting the Earth and the risk they pose to operational satellites, in the last years the interest in collecting new test data on spacecraft collisions has increased, as well as the request to improve current breakup models and develop new ones.

In this context the University of Padova performed a set of impact simulations, with a custom fragmentation algorithm, on satellites mock-ups consisting of cubic, cylindrical, and parallelepiped shapes with internal boxes representing on-board components. The considered scenarios include several targets and impactors masses and sizes and different impact geometries (in terms of velocity, impact angle and location). Simulations results consist in the generated fragments characteristic length cumulative distributions. It was observed that all distributions show different sections that can be attributed to different damage modes: the smaller fragments are generated by the spacecraft components fragmentation, the intermediate ones by the detached internal boxes, and the largest ones consisting in intact pieces of the spacecraft separated from the main structure. The limits, extent and slope of these sections depend on the impact conditions, the satellite structure and the impact point; a piecewise analytical model is derived for the simulation data, showing a good accordance with the fragments distribution trends.

Keywords: Space debris, fragmentation, breakup model

Nomenclature

EMR	Impact Energy-to-Mass Ratio, J/g
k	Correction coefficient
L_c	Characteristic length, m
m	Line slope
m_{SAT}	Satellite mass, kg
N_c	Cumulative number
α	Angle of collision, deg

1. Introduction

In less than one century of exploitation of near-Earth orbits, several fragmentation events have occurred, generating an increasing number of potentially dangerous space debris [1]. The scientific community is particularly concerned [2] about to the continuous grow of small satellites market [3] and large constellations deployment [4][5]. In fact, the probability of massive collisions among spacecraft is directly related to the number of satellites in orbit [6]; this can act as starting point for cascade events affecting the whole near-Earth environment. In addition, past episodes such as the Cosmos-Iridium one [7] showed that the generated fragments are not limited to the involved altitudes but can contaminate neighbourhood orbits.

While effective collision avoidance strategies and mitigation policies and practice can reduce the risk of in-orbit collisions [8]-[11], it is still necessary to understand the mechanisms involved in satellites collisions and identify the main parameters that might influence fragments generation. To date, the NASA Standard Breakup Model [12] is the most important tool to predict the distributions of fragments generated by collision events; in function of the impact Energy-to-Mass Ratio (EMR), the model employs the involved bodies mass or momentum as input parameter. Due to its extreme simplicity, the NASA SBM cannot distinguish between events with the same specific energy (e.g., central Vs. glancing impact). Other semi-empirical models try to address this limitation by considering the breakup dependence from collision configuration (FAST [13]), by including material properties, and by allowing to specify that certain parts of an object will remain intact after the collision (IMPACT [14]).

Identifying the main parameters that might influence satellites break-up and fragments generation is therefore important to understand this phenomenon. To date, the total number of known in-space collisions is quite limited; in addition, only a fraction of the generated fragments can be detected by ground sensors, limiting data available for this purpose. In addition, the geometry of the collision, in particular the impact point, is often unknown. This can be partially overcome by the few ground impact tests on satellites mock-ups [15]-[20]; however, in these cases the simplification of the test models (e.g., with no appendages) and the impact geometries (e.g. impacts on the centre of mock-up faces) is still limiting the identification of the parameters of interest.

To overcome this limitation, numerical simulations can be employed to evaluate a wide range of collision scenarios, evaluating the influence of different impact parameters. In this context, the Collision Simulation Tool Solver (CSTS) is a semi-empirical code simulating collisions involving satellites and providing statistically accurate fragments distributions with a low computational effort [21]. Among its applications, CSTS was employed to study the potential fragmentation of ENVISAT [22] and LOFT [23]; in the latter case, simulations investigated the effect of projectile size and point of impact, suggesting that the NASA SBM overpredicts the fragments for glancing impacts and small impactors. The validation of CSTS algorithms was performed through comparison with ground tests data, both for simple targets (up to 6 km/s) and complex configurations (up to 3.6 km/s) [21]; for conditions outside this validated range (e.g. higher impact velocities), the performed simulations campaigns still provided results consistent with the limited observation and literature data (e.g. fragments number increase with projectile mass and velocity).

On these bases, a more accurate investigation of the parameters influencing spacecraft collisions is performed with CSTS. The main objective of the simulation campaign is the investigation of the effect of geometry (velocity, impact angle, impact point) on collisions of spherical projectiles with plates and complex targets (satellites mock-ups with cubic, parallelepiped and cylindric shapes). In this phase both target and impactors are made in aluminium; the investigation of the effect of different materials (e.g., composites) is still running, as well as the analysis of scenarios with complex impactors.

This paper is organized as follows. Next section introduces the simulation plan, followed by a description of the geometries of the targets. A summary of the main simulation results follows, in terms of fragments characteristic length cumulative distributions. Last, the main parameters influencing distributions trends are discussed and a piecewise distribution model is introduced.

This work is performed in the framework of the ESA-funded project "Exploiting numerical modelling for the characterization of collision break-ups" (ESA AO 10305), in which CISAS participates in collaboration with SpaceDys (a spin-off company of the University of Pisa).

2. Simulation plan

In this section the simulation plan for this activity is presented. The CSTS software [21] is accurate and less computationally intensive with respect to the commonly available hydrocodes; however, particular care was applied in determining the parameters under investigation, in order to keep the number of simulations under control.

The parameters of interest in this campaign include:

- shape and structure of the target
- size of the spherical projectile
- impact point
- angle of collision
- impact velocity
- internal structure

The simulation plan can be seen in Table 5 in Appendix 1; it consists in 22 different impact scenarios. A first assessment of the effect of impact point, impactor shape, and target mass, size and material is performed assuming a simple shape for the target (a cube, SIM 1-14), populated with a given number of internal components (see Figure 1, top left). Following this first geometry, few additional elementary shapes were selected: a parallelepiped (populated with internal boxes, SIM 20-23, see Figure 1, top right), a flat plate (SIM 24-29, see Figure 1, bottom left), and a cylinder (populated with internal boxes, SIM 30-34, see Figure 1, bottom right). The impact geometry is also varied in this study; considering the involved geometries, the following impact points were selected:

1. central impact on a face of the target;
2. off-center impact on an edge of the target;
3. impact on the side of the cylinders (mid position);
4. impact on the base of the cylinders (close to the center).

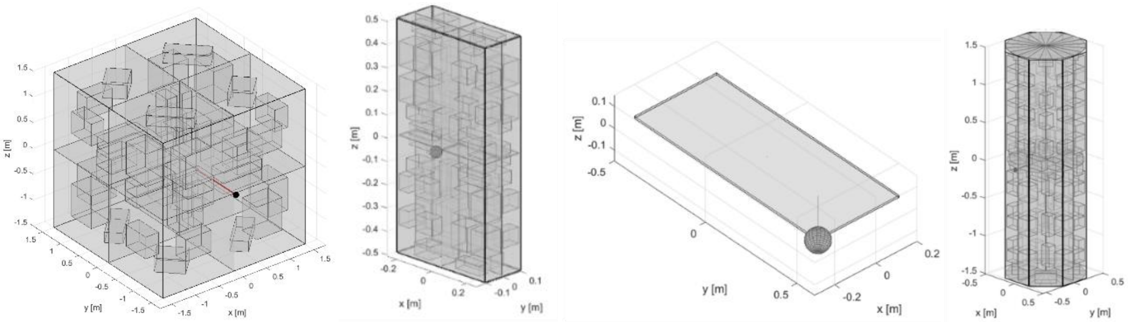

Figure 1: Target shapes for the simulated scenarios, from top to bottom, left to right: cube with internal components, parallelepiped with internal components, flat panel, cylinder with internal components.

With respect to cubic targets, they were divided in three size classes: cubes with edges of 50, 150 and 300 cm. In each size class, different target masses were imposed, to assess the effect of different internal density distributions on the generated fragments. The variation was performed keeping the target model geometry and internal distribution fixed and adjusting only the internal boxes density. The impactor masses were 0.18 kg or 1 kg. Different impact velocities allowed EMRs between 1 and 735 J/g, to investigate fragmentations below and above the commonly accepted threshold of 40 J/g that discriminates between sub-catastrophic and catastrophic impacts. For all different configurations, the influence of impact geometry (impact angle and impact point) is evaluated with dedicated simulations.

With respect to the parallelepiped (SIM 20-23) and the flat plate (SIM 24-26) targets, the geometry is fixed and the influence of the impact conditions are investigated, with EMRs respectively of 24 and 97 J/g (below and above the catastrophic fragmentation threshold of 40 J/g) and 402 and 3281 J/g (well above the catastrophic fragmentation threshold).

Last, for the cases with cylindrical targets (SIM 30-34), the geometry and the impact velocity (10 km/s) are fixed and different impactor masses (0.18 kg and 1 kg) and impact points are investigated; EMRs are respectively of 9 and 73 J/g, the latter above the catastrophic fragmentation threshold.

3. Simulation models

This section reports an overview of the geometrical models generated for this simulation campaign. For each simulation group the models are described and their main characteristics are listed and compared.

In general, the structure of the targets is composed by external and internal plates and solid boxes, representative of electronics, instrumentation and subsystems. The plates material is aluminium. Internal boxes are divided in two families: with fixed density (to be maintained equivalent in scenarios with same target geometry and different masses) and with adjustable density (to adjust the mass in scenarios with same target geometry and different masses). In case of scaled geometries, the internal distribution is always maintained. Last, structural links are provided between the internal elements, to simulate the connections and the joints among components and with structural panels.

As reported in the simulation plan Table 5, the first family of collision scenarios investigated in this campaign has a cubic target with internal boxes. Three different sizes (edges of 50, 150 and 300 cm) are considered, to investigate size effect in collisions; the target mass varies from 25 kg to 50 kg and 100 kg for the smaller size, to evaluate the effect of the equivalent density in fragments generation. Figure 2 shows the three models, including the simulation cases in which they are employed.

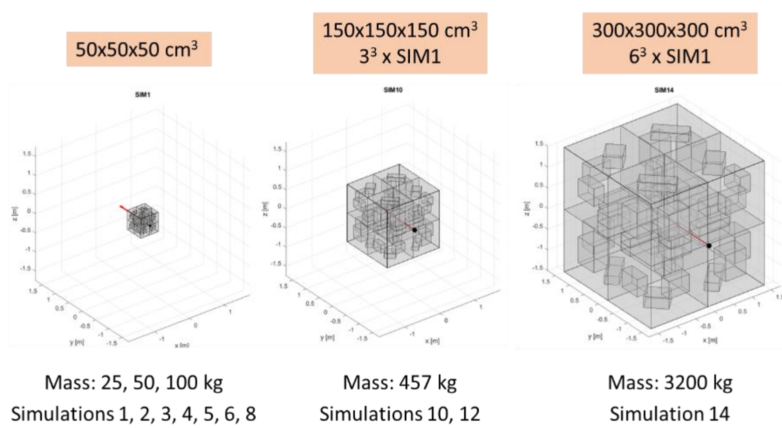

Figure 2: Cubic-shape targets with internal components

The second family of collision scenarios involve a parallelepiped target (Figure 3, left). In this case the mass and the geometry are fixed for all the considered simulations (SIM 20-23). Similarly, the third family of simulations involve a solid flat plate as target (Figure 3, right, SIM 24-26).

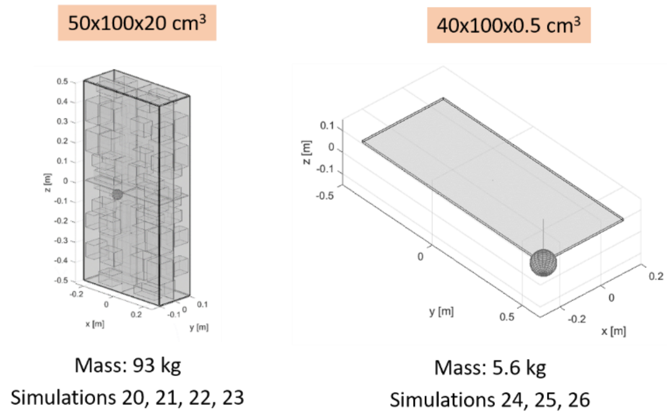

Figure 3: Parallelepiped-shape targets with internal components (left) and flat plate (right)

The fourth and last family of simulations involve aluminium cylinders (with internal boxes) as targets. Figure 4 shows model employed for simulations 31 to 34; in all cases the geometry and the mass of the target are kept constant and only the impact conditions change. Cylinders are modelled in CSTS as octagonal prisms, approximating their lateral face with eight flat plates; this helps in simplifying the fragmentation model, with a consequent reduction of simulation times.

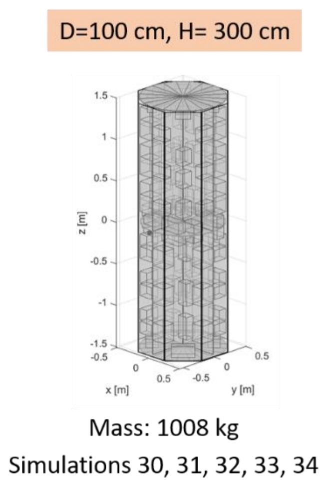

Figure 4: Aluminium cylinder shape with internal components (left) and steel cylinder (right)

4. Simulation results

In this section the main simulation results are presented and discussed. Simulations outputs are shown in terms of characteristic length distributions. The characteristic length is intended as the arithmetic mean of (*a*) the longest dimension of the object, (*b*) the longest dimension of the object measured normal to the direction of *a*, and (*c*) the longest dimension of the object normal to these two directions [24].

4.1. Sensitivity to resolution

Before starting the simulations campaign, a study on SIM 1 was performed to evaluate the sensitivity of the results to the model. The resolution is defined by a threshold size: objects with an average dimension larger than this threshold are tracked and propagated by the software; smaller debris are grouped in "bubble" objects collectively treated as a cloud of dust. Figure 5 shows the comparison of characteristic length distributions for SIM 1 for a resolution of 0.5 mm (black circles) and 1 mm (blue squares). It can be noted that the difference is negligible for fragments larger than 2 mm. The simulation time for the two cases is respectively of 23 h (resolution of 0.5 mm) and 12 h (resolution of 1 mm). In order to reduce the computation time and provide results for a first round of analysis, a resolution of 1 mm was chosen for all simulations.

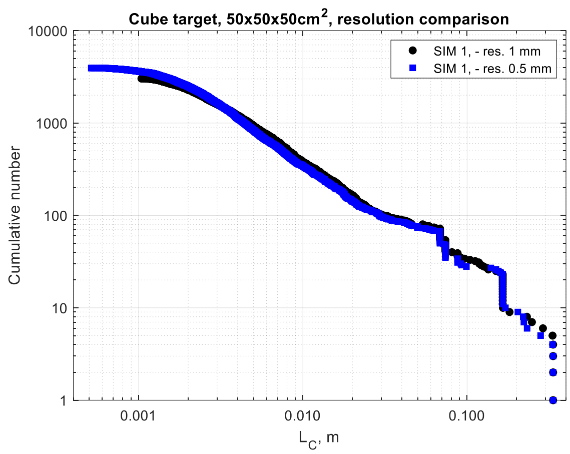

Figure 5: Comparison of characteristic length distributions for two different simulations resolutions

4.2. Target: Cube

For the first family of simulations (cubes populated with boxes as targets, aluminium spherical projectiles), Table 1 summarizes the target and impactor size and mass and the main impact parameters. In the remainder of the document, the colour and marker code defined in the table will be employed for all the plots.

Table 1: summary of simulations with cube as target

Sim. ID	Target		Projectile	Impact parameters				Colour code
	Edge (cm)	Mass (kg)	Mass (kg)	Velocity (km/s)	Impact angle	Impact Point	EMR (J/g)	
SIM-1	50	25	0.18	10.00	0°	Centre	360	
SIM-2	50	25	0.18	10.00	0°	Edge	360	
SIM-3	50	25	0.18	10.00	45°	Centre	360	
SIM-4	50	50	0.18	10.00	45°	Edge	180	
SIM-5	50	50	0.18	10.00	0°	Centre	180	
SIM-6	50	100	1.47	10.00	0°	Centre	735	
SIM-8	50	100	0.18	1.00	0°	Centre	1	
SIM-10	150	457	1.47	10.00	0°	Centre	161	
SIM-12	150	457	1.47	10.00	45°	Centre	161	
SIM-14	300	3200	1.47	10.00	0°	Centre	23	

Simulations from 1 to 8 have the same target size and geometry but different mass and impact conditions; Figure 6 shows the characteristic length cumulative distributions for these scenarios. In all the scenarios it can be noted that the fragments distributions can be divided in three different sections: residual large parts of the target, not involved in the collision (fragments larger than about 15 cm, green background), components and elements detached by the target due to the failure of structural links and joints (fragments between 4 and 15 cm, yellow background), and all the debris generated by the fine fragmentation of the elements involved in the collision (smaller than 4 cm, red background). It can be noted that the distribution of the largest fragments is only partially affected by the different impact parameters in all the evaluated scenarios.

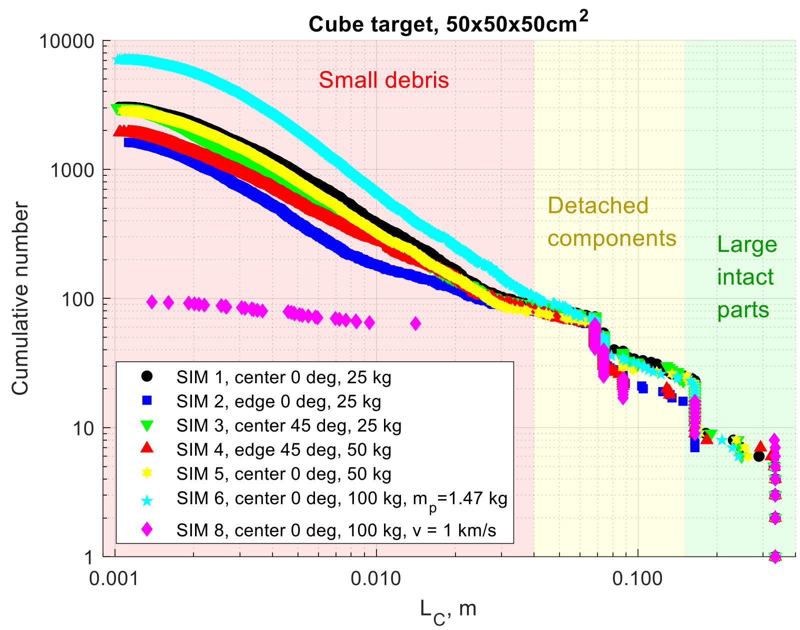

Figure 6: Comparison of characteristic length distributions for cubic targets with size 50x50x50 cm^3; where not otherwise specified, m_p=0.18 kg, v=10 km/s

For all simulations in Figure 6, it can be noted that the total number of fragments is related to the EMR value: SIM 8 (EMR=1 J/g, purple in figure) shows less than 100 fragments, SIM 6 (EMR=735 J/g, cyan) reaches 7091 fragments, while the other simulations (EMRs between 180 and 360) generate from 1600 to about 3000 fragments. The influence of the impact point and impact angle can be noted comparing SIM 1 (central impact at 0 deg, black) with SIM 2 (blue – edge impact) and SIM 3 (green – central impact at 45 deg): while the shapes of the curves are similar, the total number of fragments significantly decrease with an impact on the edge, in particular for characteristic lengths below 30 cm, and is slightly reduced for an impact at 45 deg, even for simulations with the same EMR. This result confirms the existence of a dependence between impact geometry (e.g. the fraction of the target involved in the event) and fragments generation. The effect of the target mass can be observed comparing SIM 1, black circle and SIM 5, yellow hexagram, that present the same impact conditions and masses respectively of 25 and 50 kg: while the two trends are similar, the heavier target shows a slightly lower number of fragments (about 7% less).

Figure 7 shows characteristic length cumulative distributions for the remainder of the cube targets (i.e., with larger edge sizes). Results are compared to SIM 6 (cyan, size of 50x50x50 cm^2) to evaluate the effect of target size on fragments distribution; all simulations have the same impactor (1.47 kg sphere) and collision velocity (10 km/s). Again, in all scenarios it can be noted that the fragments distributions can be divided the three different sections previously introduced: large intact parts of the target, detached components and elements, and smaller debris. In these distributions it can be noted that the transition points between the three sections translate in function of target and internal component sizes.

Considering the small fragments (characteristic lengths < 5 cm), it can be noted that the distributions are comparable for all simulations. This result suggests that for similar impact conditions (central impact point, same projectile mass and velocity) the size of the target would influence only the size of few larger (and massive) objects, while the majority of the smaller fragments will be comparable among the scenarios.

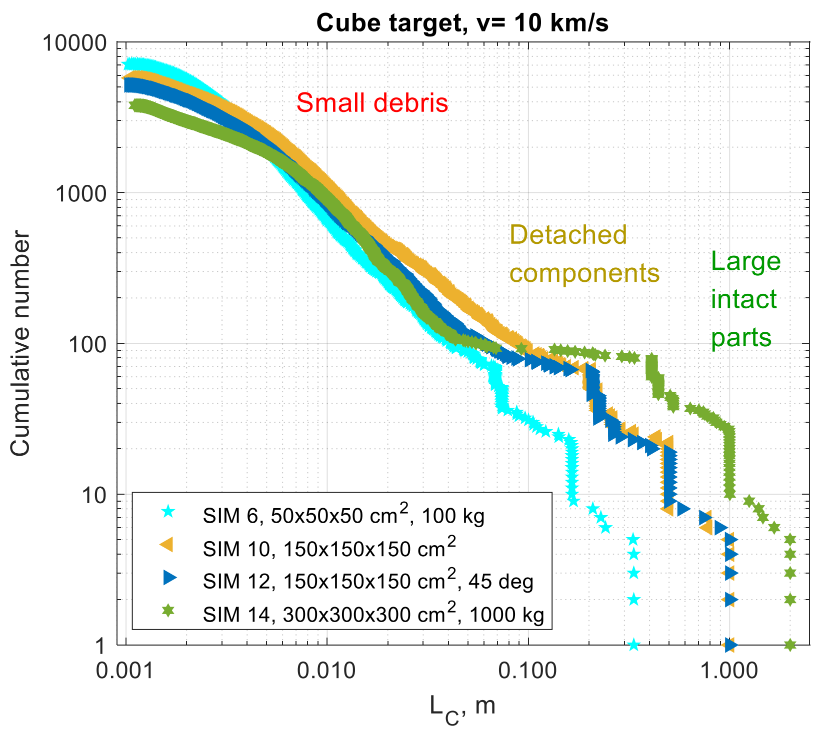

Figure 7: Comparison of characteristic length distributions for cubic targets of different sizes; where not otherwise specified, m_t=457 kg, impact at 0 deg.

4.3. Target: Parallelepiped

For the second family of simulations performed in this campaign (parallelepipeds populated with boxes as targets, aluminium spherical projectiles), Table 2 summarizes the target and impactor size and mass and the main impact parameters; the target is the same for all the scenarios (size of 50x100x20 cm^3, mass of 93 kg).

Table 2: summary of simulations with parallelepiped as target

Sim. ID	Projectile mass (kg)	Impact parameters				Colour code
		Velocity (km/s)	Impact angle	Impact point	EMR (J/g)	
SIM-20	0.18	10	0°	Centre	97	
SIM-21	0.18	5	70°	Centre	24	
SIM-22	0.18	5	0°	Edge	24	
SIM-23	0.18	5	45°	Edge	24	

Characteristic length cumulative distributions are shown in Figure 8 for the four scenarios. In general, the four curves have a similar trend, with the transition points between different fragments sources (intact parts of the target, detached components, and debris from fine fragmentation) recognizable at around 20 cm and 5 cm. The effect of the impact point (center on SIM 20 and 21, edge on SIM 22 and 23) and angle (0 deg for SIM 20 and 22, 45 deg for SIM 23, 75 deg for SIM 21) is minor on the trends and can be detected only in the range 1-5 cm; this can be related to the small size of the projectile with respect to the target dimension.

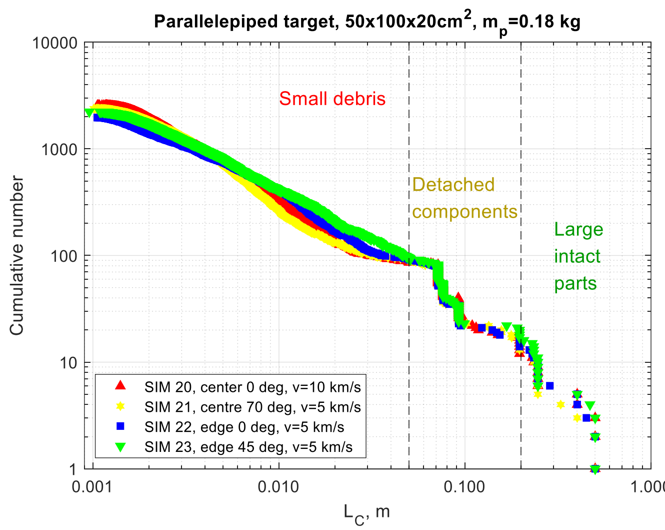

Figure 8: Comparison of characteristic length distributions for parallelepiped targets in group A

4.4. Target: Simple plate

For the third family of simulations (aluminium flat plates, aluminium spherical projectiles), Table 3 summarizes the target and impactor size and mass and the main impact parameters; the target is the same for all the scenarios (size of 40x100x0.5 cm^3, mass of 5.6 kg).

Table 3: summary simulations with flat panel as target

Sim. ID	Projectile mass (kg)	Impact parameters				Colour code
		Velocity (km/s)	Impact angle	Impact Point	EMR (J/g)	
SIM-24	0.18	5.00	0°	Centre	402	
SIM-25	0.18	5.00	45°	Centre	402	
SIM-26	1.47	5.00	0°	Edge	3281	

Figure 9 shows the characteristic length cumulative number distribution for the three simulations. It can be noted that SIM 24 (normal impact, black) and SIM 25 (impact at 45 deg, blue) have a similar trend; both scenarios have the same EMR of 402 J/g. On the contrary, a larger impactor collides with the panel on one edge in SIM 26 (green), leading to a larger EMR (3281 J/g); in this case, the total number of fragments is comparable to the previous cases and the only significant difference arises in the range between 2 mm and 4 cm, with up to an order of magnitude of more fragments.

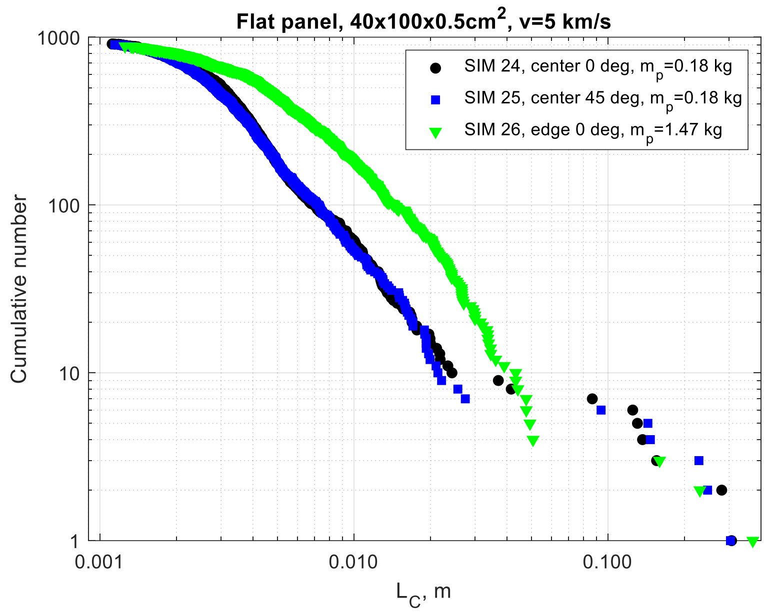

Figure 9: Comparison of characteristic length distributions for flat panels

4.5. Target: Cylinder

For the fourth family of simulations (cylinders populated with boxes, aluminium spherical projectiles), Table 4 summarizes the target and impactor size and mass and the main impact parameters; the target is the same for all the scenarios (diameter of 100 cm, height of 300 cm, mass of 1008 kg).

Table 4: summary of simulations with cylinder as target

Sim. ID	Projectile mass (kg)	Impact parameters				Colour code
		Velocity (km/s)	Impact angle	Impact point	EMR (J/g)	
SIM-30	1.47	10.00	0°	Centre	73	
SIM-31	0.18	10.00	45°	Centre	9	
SIM-32	0.18	10.00	0°	Edge	9	
SIM-33	1.47	10.00	0°	Centre of base	73	
SIM-34	0.18	10.00	0°	Centre	9	

The characteristic length distributions for this family of simulations can be seen in Figure 10. Similarly to previous complex targets (cube and parallelepiped populated with internal boxes), in all scenarios it can be noted that the fragments distributions can be divided in three different sections: fragments larger than about 60 cm (residual large parts of the target, not involved in the collision), the objects between 13 and 60 cm (components and elements detached by the target due to the failure of structural links and joints), and all the debris smaller than 13 cm (generated by the fine fragmentation of the elements involved in the collision).

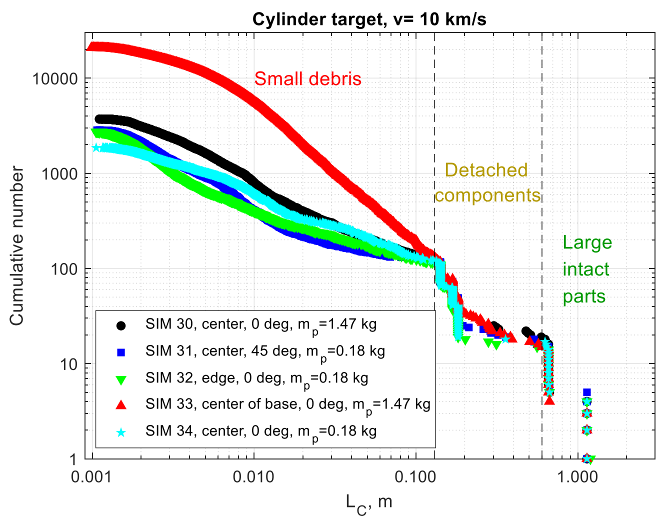

Figure 10: Comparison of characteristic length distributions for cylinder targets

In SIM 30 (black) and SIM 33 (red) the same impactor (1.47 kg spherical aluminium projectile) and the same velocity (10 km/s) are used; in this case the effect of the impact point (center of the cylinder side for SIM 30, center of its base for SIM 33) is clearly visible, with the generation of more than five times more fragments in the latter case (3709 objects for SIM 30, 20804 for SIM 33). In this case the geometry of the target strongly influences the fragments generation: in case of a normal collision on the base of the cylinder (as in SIM 33), the fraction of the target mass involved in the impact is larger than in the lateral impact scenario (such as in SIM 30); the impactor (and the debris cloud generated in the first collision) will therefore encounter a large number of objects on its trajectory through the target.

With respect to the other scenarios, it can be noted that all curves have a similar trend. The effect of projectile size can be appreciated comparing SIM 30 (1.47 kg, diameter of 10 cm) with SIM 34 (cyan, 0.18 kg, diameter of 5 cm): while for large fragments (> 10 cm) the distributions are similar, for smaller fragments SIM 34 generates less debris (1851) than SIM 30 (3709).

4.6. Comparison of different targets

In addition to the previous analysis, different targets with similar impact conditions (but with different target sizes, masses, and geometries) can be compared to investigate the influence of target geometry on fragments generation. In particular, SIM 1 (50x50x50 cm3 cube target), SIM 20 (50x100x20 cm2 parallelepiped target), and SIM 34 (cylinder target wit D=100 cm and H=300 cm) are subjected to the same impact conditions (0.18 kg impactor colliding at 10 km/s on the centre of one face). Figure 11 shows cumulative number as function of characteristic length for these scenarios: it can be noted that the different geometry is influencing not only the number and the size of the largest fragments (i.e. intact parts of the target and elements and components detached by the structure), but also the distribution of smaller fragments. In particular, it can be noted that SIM 34 (cylinder, cyan) has a lower number of total fragment but, in general, a high number of objects for sizes larger than 5 cm.

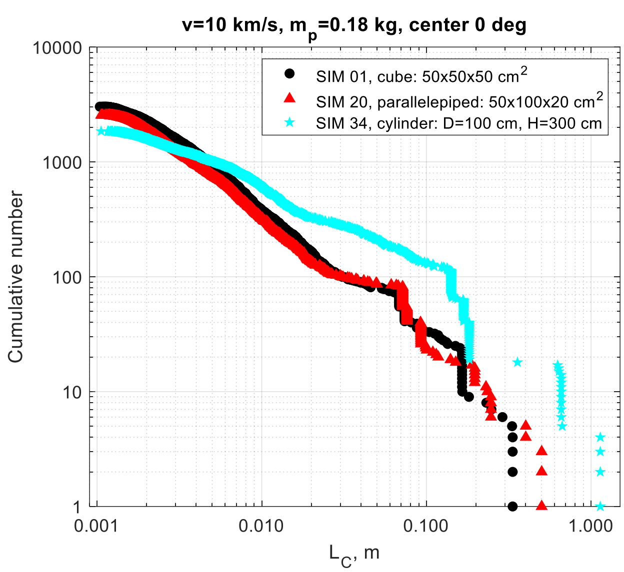

Figure 11: Comparison of characteristic length distributions for SIM 01, SIM 20, and SIM 34

4.7. Discussion

Simulations results give a general overview of the response of different geometries to collisions with simple impactors (spherical projectiles). In general, it was observed that:adobe

- The characteristic length distributions of fragments generated by CSTS can be divided in three main groups: larger fragments, representative of parts of the target that remain intact, components and elements that detach from the target structure, and small debris generated by the fine fragmentation of the parts that are directly involved in the event.
- A relationship between the characteristics of target and impactors and the number and shape of the distribution is clearly visible in the compared cases.
- In general, results suggest a relation between the geometry of the impact (impact point and direction, objects size) and fragments distributions, that could be associated to the fraction of the target directly involved in the fragmentation process.

In addition to the previous comments, a particular trend can be noted for the smaller debris class (i.e., the fragments generated by the finer fragmentation of the parts directly involved in the event). Referring to Figure 11, this section can be further divided in two quasi-linear parts: a steeper distribution of the smaller fragments and a lower slope up to the transition to the detached components section.

4.8. Piecewise distribution model

The analysis of characteristic length distributions suggests that a novel piecewise analytical model could be generated. The model, represented in Figure 12, is identified by the three branches (from 1 to 3) and the two points A (between the first and second branches) and B (between the second and third branches). The first branch includes the largest and intermediate fragments (i.e., intact parts of the target and components detached from the satellite); the second and the third parts represent the finer fragments. In this section the main parameters that influence the trend of the three sections are introduced and a first formulation of the model is proposed.

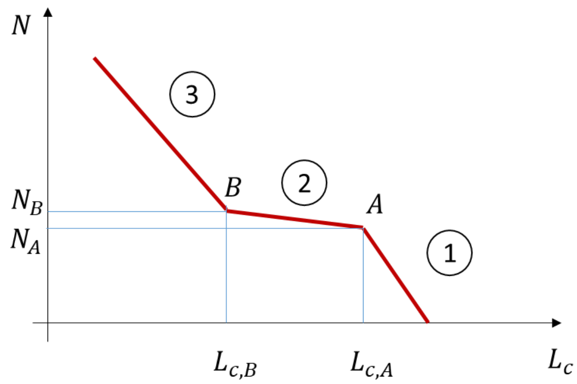

Figure 12: Three-section piecewise model, with its branches identified with the numbers from 1 to 3 and the notable points A and B.

As for the first branch, identified by the number 1, a dedicated analysis showed that for many datasets the trend of the largest fragments is quite consistent with the slope of the NASA SBM. The fragments present in this first branch are representative of parts of the satellite that have remained partly intact and a direct relationship between the size of the satellite and the position of point A has been sought. The observation of the datasets has therefore allowed defining the abscissa of point A based on the characteristic length of the satellite; the ordinate of point A is similarly related to the mass of the satellite:

$$L_{c,B} = L_{c,SAT}/10 \qquad (1)$$

$$N_{c,A} = \frac{355}{\log_{10}(m_{SAT} \cdot 1000)} \qquad (2)$$

$$m_1 = -1.71 \qquad (3)$$

Last, m_1 is the slope of the first branch and is the same as the NASA SBM.

As for the second branch, the identification of the coordinates of point B is sufficient to trace the representative segment of the distribution. Again, the abscissa of point B is based on the characteristic length of the satellite.

$$L_{c,B} = L_{c,SAT}/30 \qquad (4)$$

The ordinate of point B is also defined according to the impact parameters. In general, a relationship can be noted between the number of fragments and the specific energy of the impact (defined by the EMR parameter, which identifies how "energetic" the impact is), the equivalent density of the satellite (the ratio of its mass m_{sat} to the cube of its characteristic length $L_{C,sat}$, which gives an idea of how "compact" the satellite is) and the angle of impact α (which helps to represent how much fraction of the collision "involves" the satellite). The formulation of the ordinate of B thus becomes:

$$N_{c,B} = N_{c,A} + \Delta N_{C,B} \qquad (5)$$

$$\Delta N_{C,B} = 10 \cdot \log_{10}(EMR \cdot 1000) \cdot \cdot \log_{10}\left(\frac{m_{SAT}}{L^3_{c,SAT}}\right) \cdot \cos(\alpha) \cdot k \qquad (6)$$

To consider edge impacts, the corrective coefficient k is also included. The values of k are between 1 (impact passing through the centre of mass of the satellite) and 0 (glancing impact). As reference, an edge impact normal to one of the faces is evaluated as 1/3, an edge impact directed through the inside of the target has a coefficient k larger than this value, while an impact near one edge and directed “outside” the target is evaluated lower than 1/3. We want to emphasize that in the current model the dependence on the angle of impact and on the coefficient k is representative of the "mass fraction" of the satellite directly involved in the impact. In future refinements of the model, it is planned to replace this parameter with a "coefficient of mass involved", defined as a function of the point of impact and the ratio between the mass of the sections of the target and the impactor involved in the collision and the total mass of the system.

Last, the third and final branch is defined by the point B and the inclination of the curve. In this case the slope was modeled with a formulation linked to the initial value proposed by the NASA SBM (-1.71) and to the EMR and mass parameters of the satellite:

$$c_1 = \max\left(1, \log_{10}\left(\frac{m_{SAT}}{10}\right)\right) \qquad (7)$$

$$c_2 = \log_{10}(10 \cdot EMR) / c_1 \qquad (8)$$

$$m_3 = 0.75 \cdot \begin{cases} 0 & c_2 < 0 \\ -1.71 \cdot c_2 & 0 \le c_2 < 1 \\ -1.71 & c_2 \ge 1 \end{cases} \qquad (9)$$

In addition, collision scenarios with very-low EMRs (below 10 J/g) are corrected with a scaling parameter:

$$m_3' = m_3 \cdot \frac{EMR}{10} \qquad (10)$$

$$\Delta N_{C,B}' = \Delta N_{C,B} \cdot \frac{EMR}{10} \qquad (11)$$

Comparing this model with literature, it is worth to notice that a relation between the cumulative distribution slope and the logarithm of the EMR has been already introduced for fragments mass distributions in the IMPACT algorithm, as well as the concept of mass fraction [25]. In addition, the 10 J/g threshold was already and independently proposed for the same model as a lower boundary for the transition from complete to highly incomplete fragmentation [26].

Figure 14 compares simulation results with the piecewise model. It can be noted that for all cases the model is capable to represent the fragments distribution trend. Among the results, only SIM 14 (largest and heaviest cubic target) is strongly overestimated by the model.

A particular attention should be given to SIM 33 (cylindric target, impact on base). In this case, the “mass fraction” involved in the event is clearly larger with respect to the other scenarios involving cylindric targets impacted on their lateral faces. Considering that the ratio between the cylinder radius and its height is 3, for this scenario such value is assumed for the corrective coefficient *k*. Figure 13 shows SIM 33 simulation data in comparison with the piecewise model with and without the correction. It can be observed that the corrected distribution is more representative of the numerical data. This is a further strong suggestion that the “mass fraction” involved in the collision shall be considered in future refinements of this model.

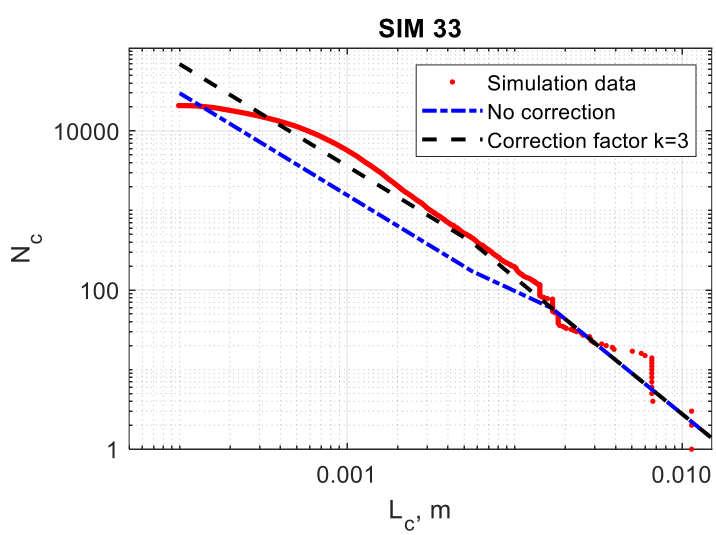

Figure 13: SIM 33: comparison of simulation data with piecewise model, without and with a correction factor *k*.

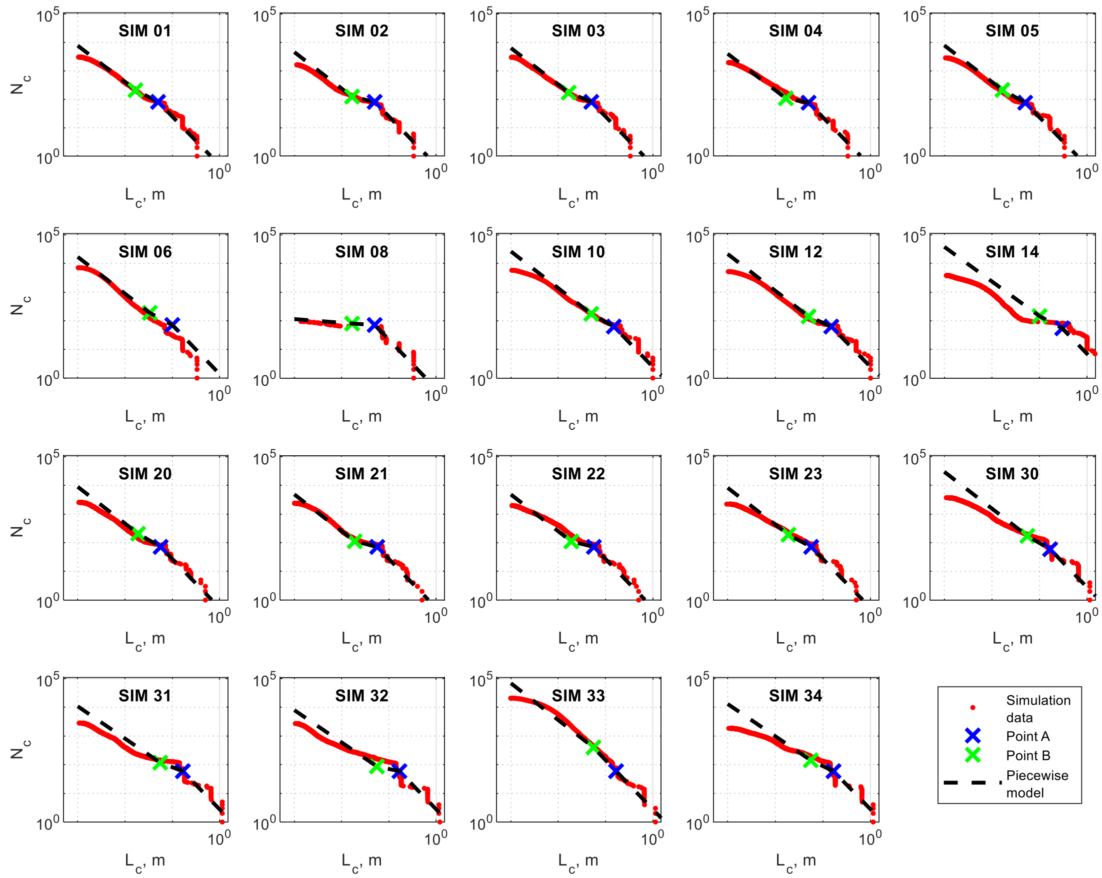

Figure 14: Comparison between simulation data and piecewise distribution model

5. Conclusions

In this document a summary of a simulation campaign on multiple scenarios of in-orbit collision was reported, highlighting the main results in terms of fragments characteristic length distributions. A total of 22 simulations were performed, focusing on aluminium targets and simple aluminium impactors.

In general, it was observed that the characteristic length distributions of fragments generated by CSTS can be divided in three main groups: larger fragments, representative of parts of the target that remain intact, components and elements that detach from the target structure, and small debris generated by the fine fragmentation of the parts that are directly involved in the event. Fragments distributions are strongly influenced by the impact geometry (and therefore the “mass fraction” of the target involved in the collision).

A piecewise model was elaborated following these considerations. It consists in three branches, which parameters are related to the impact EMR, the satellites models size and mass, and the impact geometry; for low EMRs (below 10

J/s) a scaling correction is employed. The model represents the simulation data trends with enough accuracy; its formulation suggests the importance of the "mass fraction" involved in the collision in fragments generation.

To expand the validity of these results, further simulations are running to evaluate the influence of target material (e.g., CFRP instead of aluminium) on fragments generation. In parallel, more complex scenarios involving larger impactors with internal components distributions are under scrutiny. In the future, it is planned to compare simulations results with experimental and observation data to obtain a wider dataset. This information will be important to further improve the proposed novel analytical satellite breakup model by including all the parameters affecting in-orbit collisions.

Acknowledgements

This work is performed in the framework of ASI-INAF contract n. 2020-6-HH.0 "Detriti Spaziali - Supporto alle attività IADC e SST 2019-2021". The simulations presented in this this work were performed for ESA contract n. TDE-T711-603SD "Exploiting numerical modelling for the characterisation of collision break-ups".

References

[1] Kessler, D. J., & Cour-Palais, B. G. (1978). Collision frequency of artificial satellites: The creation of a debris belt. *Journal of Geophysical Research: Space Physics*, **83**(A6), 2637-2646.

[2] Radtke, J., Kebschull, C., Stoll, E. (2017). Interactions of the space debris environment with mega constellations—using the example of the oneweb constellation. *Acta Astronaut.* **131**, 55–68.

[3] Karacalioglu, A. G., & Stupl, J. (2016). The Impact of New Trends in Satellite Launches on the Orbital Debris Environment. *NASA Technical Report. Houston, TX, United States* (2016)

[4] Virgili, B., Dolado, J., Lewis, H., Radtke, J., Krag, H., Revelin, B., Cazaux, C., Colombo, C., Crowther, R., Metz, M. (2016). Risk to space sustainability from large constellations of satellites. *Acta Astronaut.* **126**, 154–162.

[5] Olivieri, L., & Francesconi, A. (2020). Large constellations assessment and optimization in LEO space debris environment. *Advances in Space Research*, **65**(1), 351-363.

[6] Lewis, H.G., Radtke, J., Rossi, A., Beck, J., Oswald, M., Anderson, P., Bastida Virgili, B., Krag, H. (2017). Sensitivity of the space debris environment to large constellations and small satellites. In: *Proc. 7th European Conference on Space Debris*, Darmstadt, Germany.

[7] McKnight, D., Di Pentino, F., & Knowles, S. (2014). Massive Collisions In LEO - A Catalyst To Initiate ADR. In: *Proc. 65th International Astronautical Congress*, Toronto, CA.

[8] Kawamoto, S., Nagaoka, N., Sato, T., & Hanada, T. (2020). Impact on collision probability by post mission disposal and active debris removal. *Journal of Space Safety Engineering*, *7*(3), 178-191.

[9] Colombo, Camilla, et al. "Effects of passive de-orbiting through drag and solar sails and electrodynamic tethers on the space debris environment." 69th International Astronautical Congress (IAC 2018). International Astronautical Federation, IAF, 2018.

[10] Rossi, Alessandro, et al. "ReDSHIFT: A global approach to space debris mitigation." Aerospace 5.2 (2018): 64.

[11] Tadini, Pietro, et al. "Active debris multi-removal mission concept based on hybrid propulsion." Acta Astronautica 103 (2014): 26-35.

[12] Johnson, Nicholas L., et al. "NASA's new breakup model of EVOLVE 4.0." *Advances in Space Research* 28.9 (2001): 1377-1384.

[13] D. McKnight, R. Maher, L. Nagl, Refined algorithms for structural breakup due to hypervelocity impact, Int. J. Impact Eng. 17 (1995) 547–558.

[14] M.E. Sorge, D.L. Mains, IMPACT fragmentation model developments, Acta Astronaut. 126 (2016) 40–46.

[15] Hanada, T., Liou, J. C., Nakajima, T., & Stansbery, E. (2009). Outcome of recent satellite impact experiments. *Advances in Space Research*, *44*(5), 558-567.

[16] Lan, S. W., Liu, S., Li, Y., Ke, F. W., & Huang, J. (2014). Debris area distribution of spacecraft under hypervelocity impact. *Acta Astronautica*, *105*(1), 75-81.

[17] Abdulhamid, H., Bouat, D., Collé, A., Lafite, J., Limido, J., Midani, I., ... & Omaly, P. On-ground HVI on a nanosatellite. Impact test, fragments recovery and characterization, impact simulations. In: Proc. 8th European Conference on Space Debris, Darmstadt, Germany

[18] Olivieri, L., Smocovich, P. A., Giacomuzzo, C., & Francesconi, A. (2022). Characterization of the fragments generated by a Picosatellite impact experiment. *International Journal of Impact Engineering*, *168*, 104313.

[19] McKnight D, Fudge M, Maclay T (1998a). Satellite Orbital Debris Characterization Impact Test (SOCIT) Series Data Collection Report. NASA contract NAS 9-19215

[20] Liou JC, Clark S, Fitz-Coy N, Huynh T, Opiela J, Polk M, Roebuck B, Rushing R, Sorge M, Werremeyer M (2013). DEBRISAT – A Planned Laboratory-based Satellite Impact Experiment for Breakup Fragment Characterization. In: Proc. 6th European Conference on Space Debris, Darmstadt, Germany

[21] Francesconi, A., Giacomuzzo, C., Olivieri, L., Sarego, G., Duzzi, M., Feltrin, F., ... & de Wilde, D. (2019). CST: A new semi-empirical tool for simulating spacecraft collisions in orbit. Acta Astronautica, 160, 195-205.

[22] Olivieri, L., Giacomuzzo, C., Duran-Jimenez, C., Francesconi, A., & Colombo, C. (2021). Fragments Distribution Prediction for ENVISAT Catastrophic Fragmentation. In *8th European Conference on Space Debris, ESA/ESOC* (pp. 1-12). ESA.

[23] Francesconi, A., Giacomuzzo, C., Olivieri, L., Sarego, G., Valmorbida, A., Duzzi, M., ... & de Wilde, D. (2022). Numerical simulations of hypervelocity collisions scenarios against a large satellite. *International Journal of Impact Engineering*, *162*, 104130.

[24] Schonberg, William P., and Joel E. Williamsen. RCS-based ballistic limit curves for non-spherical projectiles impacting dual-wall spacecraft systems. International journal of impact engineering 33.1-12 (2006): 763-770.

[25] Mains, Deanna L., and Marlon E. Sorge. The IMPACT satellite fragmentation model. *Acta Astronautica* 195 (2022): 547-555.

[26] Sorge, Marlon. Satellite fragmentation modeling with IMPACT. *AIAA/AAS Astrodynamics Specialist Conference and Exhibit*. 2008.

Appendix A: Simulation plan

Table 5: Simulation plan with simulation ID, target and impactor characteristics, and impact parameters

Sim. ID	Target				Impactor		Impact parameters			
	Shape	Size, cm^3	Material	Mass (kg)	Shape	Mass (kg)	Vel. (km/s)	Impact angle	Impact Point	EMR (J/g)
SIM-1	Cube	50x50x50	Al-alloy	25	Sphere	0.18	10.00	0°	Centre	360
SIM-2		50x50x50	Al-alloy	25	Sphere	0.18	10.00	0°	Edge	360
SIM-3		50x50x50	Al-alloy	25	Sphere	0.18	10.00	45°	Centre	360
SIM-4		50x50x50	Al-alloy	50	Sphere	0.18	10.00	45°	Edge	180
SIM-5		50x50x50	Al-alloy	50	Sphere	0.18	10.00	0°	Centre	180
SIM-6		50x50x50	Al-alloy	100	Sphere	1.47	10.00	0°	Centre	735
SIM-8		50x50x50	Al-alloy	100	Sphere	0.18	1.00	0°	Centre	1
SIM-10		150x150x150	Al-alloy	457	Sphere	1.47	10.00	0°	Centre	161
SIM-12		150x150x150	Al-alloy	457	Sphere	1.47	10.00	45°	Centre	161
SIM-14		300x300x300	Al-alloy	3200	Sphere	1.47	10.00	0°	Centre	23
SIM-20	Parallelepiped	50x100x20	Al-alloy	93	Sphere	0.18	10.00	0°	Centre	97
SIM-21		50x100x20	Al-alloy	93	Sphere	0.18	5.00	70°	Centre	24
SIM-22		50x100x20	Al-alloy	93	Sphere	0.18	5.00	0°	Edge	24
SIM-23		50x100x20	Al-alloy	93	Sphere	0.18	5.00	45°	Edge	24
SIM-24	Flat Panel	40x100x0.5	Al-alloy	5.6	Sphere	0.18	5.00	0°	Centre	402
SIM-25		40x100x0.5	Al-alloy	5.6	Sphere	0.18	5.00	45°	Centre	402
SIM-26		40x100x0.5	Al-alloy	5.6	Sphere	1.47	5.00	0°	Edge	3281
SIM-30	Cylinder	D=100cm, H=300cm	Al-alloy	1008	Sphere	1.47	10.00	0°	Centre	73
SIM-31		D=100cm, H=300cm	Al-alloy	1008	Sphere	0.18	10.00	45°	Centre	9
SIM-32		D=100cm, H=300cm	Al-alloy	1008	Sphere	0.18	10.00	0°	Edge	9
SIM-33		D=100cm, H=300cm	Al-alloy	1008	Sphere	1.47	10.00	0°	Centre of base	73
SIM-34		D=100cm, H=300cm	Al-alloy	1008	Sphere	0.18	10.00	0°	Centre	9